

Use of self-actuating and self-sensing cantilevers for imaging biological samples in fluid

G E Fantner^{1,7}, W Schumann^{2,3,7}, R J Barbero⁴, A Deuschinger⁵,
V Todorov⁶, D S Gray¹, A M Belcher^{1,4}, I W Rangelow³ and
K Youcef-Toumi²

¹ Department of Materials Science and Engineering, Massachusetts Institute of Technology, Cambridge, MA 02139, USA

² Department of Mechanical Engineering, Massachusetts Institute of Technology, Cambridge, MA 02139, USA

³ Department of Electrical Engineering and Information Technology, Ilmenau University of Technology, D-98693 Ilmenau, Germany

⁴ Department of Biological Engineering, Massachusetts Institute of Technology, Cambridge, MA 02139, USA

⁵ ISAS—Institute for Sensor and Actuator Systems, Vienna University of Technology, A-1040 Vienna, Austria

⁶ Techproject, A-1230 Vienna, Austria

E-mail: fantner@mit.edu

Received 23 May 2009, in final form 24 July 2009

Published 2 October 2009

Online at stacks.iop.org/Nano/20/434003

Abstract

In this paper, we present a detailed investigation into the suitability of atomic force microscopy (AFM) cantilevers with integrated deflection sensor and micro-actuator for imaging of soft biological samples in fluid. The Si cantilevers are actuated using a micro-heater at the bottom end of the cantilever. Sensing is achieved through p-doped resistors connected in a Wheatstone bridge. We investigated the influence of the water on the cantilever dynamics, the actuation and the sensing mechanisms, as well as the crosstalk between sensing and actuation. Successful imaging of yeast cells in water using the integrated sensor and actuator shows the potential of the combination of this actuation and sensing method. This constitutes a major step towards the automation and miniaturization required to establish AFM in routine biomedical diagnostics and *in vivo* applications.

(Some figures in this article are in colour only in the electronic version)

1. Introduction

Imaging a wide variety of samples with nanometer resolution and in a broad range of environments (vacuum, air, fluids) is a unique feature of the atomic force microscope (AFM). Its uses range from imaging hard samples with sub-nanometer resolution, for example in process control and semiconductor fabrication [1–3], to imaging very soft samples in life sciences [4–7]. Especially in areas where samples can be imaged in air or vacuum, AFM has become an established

technique. Instrument automation has allowed high quality AFM images to be taken even by inexperienced or infrequent users [8]. AFM has also yielded many medically relevant results in a research setting [5, 9–11] on living organisms or tissues. The use of AFM on such soft biological samples in liquid, however, demands a much higher skill level from the user. This has prevented a broader use of AFM in the life sciences and medical diagnostics. A higher level of system integration, miniaturization and automation has to be developed to make AFM measurements feasible in a routine clinical setting. In this paper, we report on the use of self-actuated, self-sensing AFM cantilevers on biological samples

⁷ GEF and WS contributed equally to this work.

in liquid. These cantilevers allow easier system integration and miniaturization, provide better controllability and offer the potential for full automation.

Cantilever technology and micro-fabrication have been key driving forces for the success of AFM and its diverse uses [12]. Batch processing allowed the fabrication of cantilevers with a wide variety of stiffnesses and resonance frequencies, which are specially designed for specific applications [13–16]. Cantilevers developed for imaging in vacuum and air generally have a higher resonance frequency and spring constant ($f_0^{\text{air}} \approx 40\text{--}400$ kHz, $k \approx 1\text{--}80$ N m⁻¹). Cantilevers designed for operation in fluid and on soft samples generally have a lower resonance frequency and spring constant ($f_0^{\text{air}} \approx 10\text{--}30$ kHz, $k \approx 0.01\text{--}0.5$ N m⁻¹). The most common method to detect the cantilever deflection uses a laser beam reflected from the back of the cantilever as an optical lever [17, 18]. This method allows atomic resolution imaging [17, 19] and force detection with very low noise [20, 21], but it requires a relatively large number of additional components such as a laser, optics and detectors which require space and alignment. To circumvent the need for these components, cantilevers with integrated sensors have been developed [22]. Advances in micro-fabrication have also allowed the integration of actuators directly on the cantilever, either through piezoelectric actuation [23], magnetic actuation [24–27], mechano-thermal actuation [28] or Lorentz actuation [29]. Direct actuation reduces the need for external piezoactuators and increases the cantilever actuation speed and precision [30, 31]. Previous sensor and actuator designs have been deemed not suitable for actuation in water due to the interaction of the actuation and sensing mechanisms (with the exception of magnetic and Lorentz actuation, which can only be used for exciting the cantilever in resonance). To our knowledge, integration of deflection sensing in combination with magnetic or Lorentz actuation is problematic and has not yet been achieved. In this paper, we use AFM cantilevers with a low voltage thermo-mechanical actuator and piezoresistive deflection sensors for imaging biological samples in water. This combination of actuation and sensing within one cantilever compatible with imaging in fluid constitutes a major step towards miniaturization and automation of AFM to be used in routine clinical diagnostics or *in vivo* AFM [8].

2. Materials and methods

2.1. Cantilever, readout and actuation

For all experiments in this work, we used cantilevers with integrated thermal drive and resistive readout. The fabrication method is described by Linnemann *et al* [16], Ivanov *et al* [32] and Pedrak *et al* [28]. Figure 1(A) shows an SEM image of the silicon cantilevers with thermal heating loops made up of gold near the tip and piezoresistive elements on the cantilever base. The cantilever tip was an isotropically etched Si tip with a height of approx. 4 μm . Two types of cantilevers were used. The first type, as shown in figure 1(B), has a full Wheatstone bridge on the cantilever chip. Two of the

bridge resistors are located at the cantilever base, sensing the cantilever motion. The other two resistors are situated at the chip. The second cantilever type has only one resistor on the cantilever base. All other resistors of the Wheatstone bridge are integrated in the readout electronics. The advantage of the full bridge integration is that the resistors in the Wheatstone bridge are better matched in value and need less offset to be applied to balance the bridge. Once the bridge was balanced, no significant performance difference was observed for our measurements. The cantilevers are 320 μm in length, 110 μm in width and 3–5 μm in thickness and their spring constants vary between 2 and 11 N m⁻¹ due to fabrication. Since the spring constant is essential in determining the cantilever suitability for imaging biological samples in water, we selected the cantilevers with the lowest spring constants for our experiments, regardless of whether they had one resistor or four integrated resistors. The cantilever chips are wire-bonded to a printed circuit support chip used for the electrical and mechanical connection. For most experiments in air and water, the cantilevers were uncoated. For the experiments described in sections 2.3 and 3.3, the cantilevers were thinly coated in formvar. The cantilevers on the PC-board chip were then connected to a custom cantilever holder with integrated electronics and piezo-stack. Figure 1 shows the set-up that allows the excitation of the cantilever in resonance with either conventional tapping piezo- or thermal actuation. The cantilever holder is made of acrylic and allows optical access for optical lever deflection. The cantilever motion detection can be changed from conventional optical readout to piezoresistive readout using a single switch.

2.2. Set-up integration

The cantilever holder is used in a Multimode AFM (Veeco Metrology) connected to a Nanoscope IIIa AFM controller with basic extender. The electronics in the holder supply a voltage of 2.046 V to the Wheatstone bridge. The bridge signal is amplified by an instrumentation amplifier (AD8250, Analog Devices) and further amplified by two 10 \times gain stages (AD8022, Analog Devices). The Wheatstone bridge is balanced by an offset added to the signal after the instrumentation amplifier.

In the standard set-up the actuation signal is generated by the AFM controller (in our case a Nanoscope IIIa controller) running in tapping mode (intermittent contact mode) and accessed as a low voltage signal (in our case at the signal access module), see figure 1(D). To control the current through the thermal actuator a variable resistor (50–250 Ω) is connected in series. The piezoresistor signal coming from the readout electronics in the cantilever holder is inserted into the AFM controller and replaces the optical signal (in our case through the signal access module).

This set-up allows the measurement of the deflection of the cantilever with the optical lever detection system as well as the piezoresistive sensor. In a direct comparison of the noise performance, the piezoresistive measurement showed a factor of four more noise than the optical lever detection (the maximum noise power for the optical and the resistive sensing was 0.6 pm² Hz⁻¹ and 2.4 pm² Hz⁻¹, respectively).

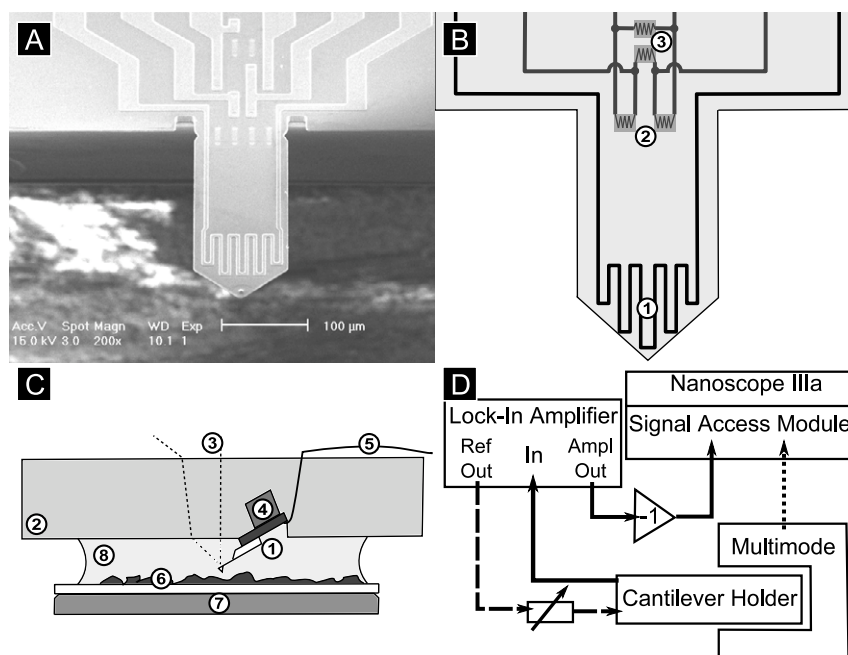


Figure 1. Active cantilever with integrated thermal actuation and piezoresistive readout. (A) SEM image of an active cantilever with integrated Wheatstone bridge. (B) Schematic of the active cantilever with thermal actuation (1) at the cantilever tip, two piezoresistors (2) detecting the cantilever's motion and the resistors (3) completing the Wheatstone bridge integrated on the chip. (C) Schematic of the experimental set-up for imaging in water: the active cantilever (1) is mounted on a Plexiglas holder (2) allowing the laser beam (3) necessary for conventional readout to pass through. Excitation is possible either with the piezoactuator (4) glued into the Plexiglas holder or with the thermal actuation on the cantilever. All electrical connections (5) to and from the cantilever pass through the holder. The sample (6) is moved in x , y and z directions by a piezotube (7). The water (8) is located between the cantilever holder and the sample. (D) Schematic connection diagram for 2ω detection. Dashed line: thermal drive signal, dotted line: optical deflection signal, solid line: resistor deflection/amplitude signal.

2.3. 2ω excitation

For the 2ω drive (see section 3.3) an eLockIn 204 lock-in amplifier (Anfatec Instruments) is used to generate the excitation signal and measure the amplitude of the resistor signal at ω and 2ω simultaneously (figure 1(D)). The signal from the readout electronics is low- and high-pass filtered by SIM 965 24 dB analog filters (Stanford Research Systems) as well as amplified by an SIM 980 summing amplifier (Stanford Research Systems) before it is processed in the lock-in amplifier. The Nanoscope IIIa controller was operated in contact mode, in order to use the PI feedback controller of the Nanoscope IIIa while performing the amplitude detection externally with the lock-in amplifier. In tapping mode, the control variable (the amplitude of the deflection signal) decreases when detecting an increase in topography. In contact mode, the control variable (the cantilever deflection) increases when detecting an increase in topography. Therefore, the amplitude signal from the lock-in amplifier was inverted before inserting into the signal access module as a deflection signal. During imaging, the deflection set-point (which acted as the inverted amplitude set-point) was chosen to be between -1 and -0.1 V. For the experiments in water with 2ω drive, we coated the active cantilevers in a 0.5% formvar solution in ethylene dichloride (electron microscopy sciences) to counteract bubble formation and electrostatic attraction of contaminants (see section 4).

2.4. Immobilizing yeast cells on polylysine covered glass

To increase adhesion between the yeast and the glass substrate, glass coverslips were coated with polylysine before depositing the yeast. Round glass coverslips were boiled in 0.2 M HCl for 10 min to clean the glass. After HCl treatment, the coverslips were rinsed 5–6 times in distilled water. Then the coverslips were immersed in 0.05 mg ml⁻¹ poly-L-lysine hydrobromide (Sigma part number: P1524), 10 mM Tris-HCl, pH 8.0 for 10 min. The coverslips were removed from the liquid and were dried overnight on end at room temperature. The coverslips were stored at room temperature and were used within one week.

Saccharomyces cerevisiae yeast cells (strain EBY100) were grown overnight at 30 °C in yeast growth media (SD-CAA) to a concentration of roughly 4.5 OD₆₀₀ ml⁻¹ as described previously [33]. Cells were stored in the growth media at 4 °C until the day of imaging. On the day of imaging, 1 ml of cells was removed and washed three times with distilled water. The cells were washed by centrifugation with subsequent removal of the supernatant. The remaining cells were then resuspended in fresh water. After the final wash, the cells were resuspended in 100 μ l of water and added to a polylysine-coated glass coverslip. The water was allowed to evaporate at room temperature (typically 1–2 h of drying time). At this point there was a thick sheet of yeast cells on the coverslip. To remove the top layers of cells, the coverslip

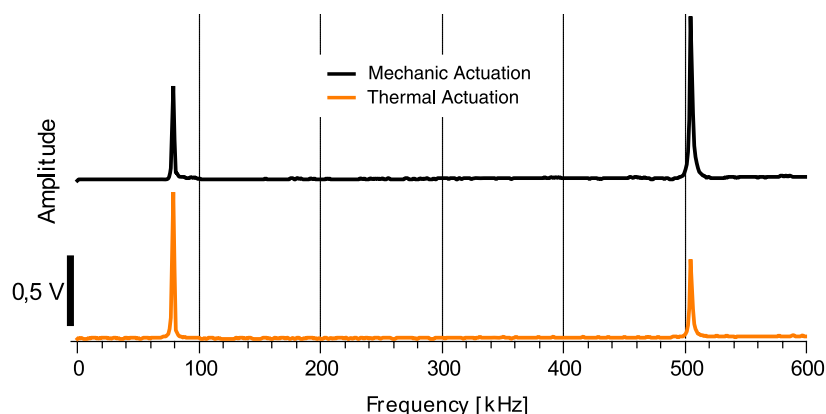


Figure 2. Tuning curves in air recorded with optical lever detection using either external inertial excitation (black line) or internal thermal excitation (red curve). The difference in relative magnitude of the first and second eigenfrequency is most likely due to a different laser alignment.

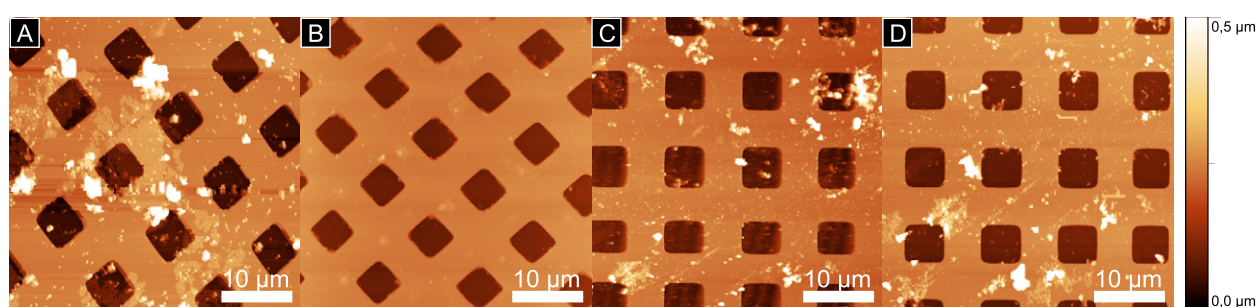


Figure 3. AFM images of a 10 μm pitch calibration grating recorded in air using the four combinations of actuation and sensing. (A) Inertial drive and optical readout, (B) inertial drive and resistor readout, (C) thermal drive and optical readout, and (D) thermal drive and resistor readout. The resolution of the AFM image is comparable between all the methods, as can be seen from the fine features of the contamination on the grating.

was washed with a micropipette and clean water. The coverslip was washed until the thick yeast layer was not visible by eye (typically requiring rinsing with 4–5 ml of water). After brief drying, the coverslip was ready for imaging on the AFM in water or in air.

2.5. Cross-linking yeast cells on AFM slides

For imaging the yeast in fluid using both thermal actuation and resistive sensing, the yeast cells were cross-linked to increase adhesion and sample rigidity. *S. cerevisiae* were grown and washed as described above. After washing, the cells were resuspended in 100 μl of 7.5% glutaraldehyde. 25 μl of this mixture was added to a polylysine-coated glass coverslip and was allowed to dry. The coverslip could then be imaged in water or in air.

3. Results

To investigate the suitability of the fully actuated cantilevers for imaging in fluid, we first established the achievable image quality on hard and soft samples in air. After this, we investigate the changes in imaging behavior and performance when the experiments are performed in fluid.

3.1. Measurements in air

First we characterized the behavior and interactions of the two different actuation methods (mechanical excitation with an external piezo-stack, and thermal actuation) and the two deflection readout methods (optical lever detection with laser and piezoresistive readout) when imaging in tapping mode (AC mode) in air. Figure 2 shows the tuning curves of one of the actuated cantilevers when actuated using the external inertial drive and the internal thermal drive. The resonance behavior is nearly identical (the difference in the relative magnitude of the first and second eigenfrequency is most likely due to a different laser alignment between the two cases, which was necessary due to the constant pre-stress which is present in the case of thermal actuation). Figure 3 shows height images of a 10 μm pitch calibration grating imaged with the four combinations of actuator and sensor. Figure 3(A) represents the standard mechanical actuation and optical lever sensing, whereas figure 3(D) represents thermal actuation and resistor sensing. The image quality of all four combinations are comparable, with a little better noise performance in the case of optical versus resistor deflection. The noise sources in the case of resistor deflection measurement consist of the intrinsic noise of the resistors in the Wheatstone bridge, the electromagnetic pickup in the Wheatstone bridge, the supply and sensing wires

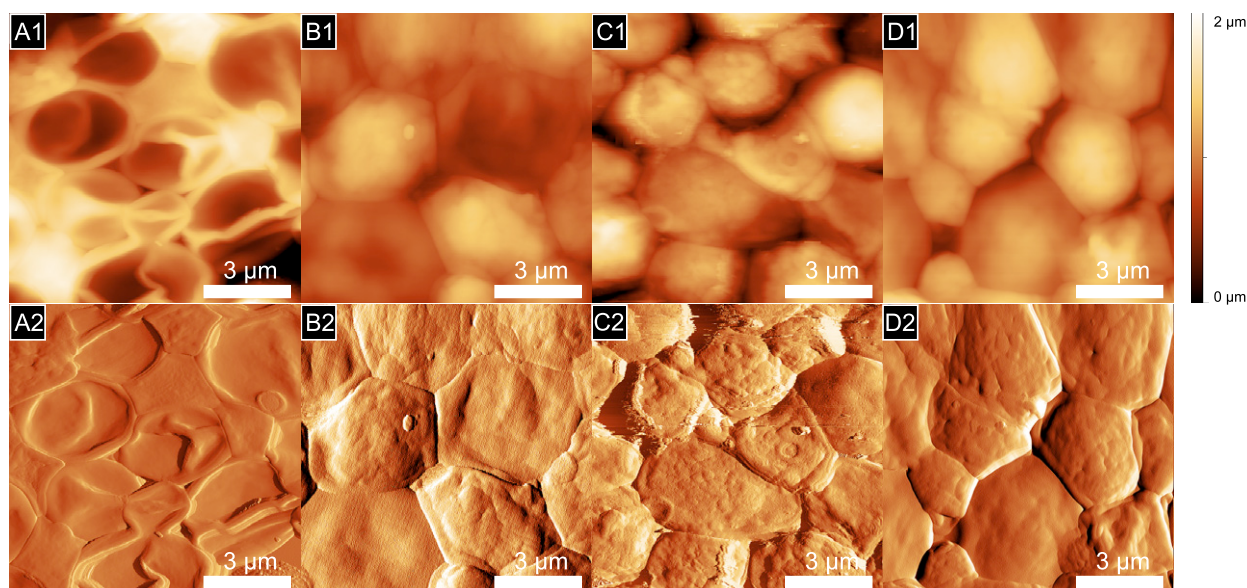


Figure 4. AFM images of yeast cells recorded in air, deposited on polylysine-covered glass slides imaged with the four combinations of actuation and sensing. Image 1 represents the height data, image 2 represents the amplitude error. (A1&2) Inertial drive, optical readout, (B1&2) inertial drive and resistor readout, (C1&2) thermal drive and optical readout, (D1&2) thermal drive and resistor readout. The surface morphology of the yeast cells can be resolved well. In the case of the resistor readout, an electrical interference from 60 Hz induction causes a slightly striped appearance in the amplitude images.

as well as noise generated by the subsequent instrumentation amplifiers and gain stages.

Figure 4 shows tapping mode images of yeast deposited on a polylysine-coated coverslip imaged in air. The differences in the appearance of the yeast in the four cases is mainly due to differences in the samples used for the different experiments. Figure 4(A), for example, shows the yeast cells collapsed and exhibiting folds in the surface. We assume that this is due to differences in dehydration and lack of support from surrounding yeast cells. Figure 4(B2) shows a periodic noise which is manifested in a striped pattern which can be attributed to 60 Hz pickup from the AC supply onto the cantilever deflection signal. Figure 4(C) shows some imaging artifacts, which we attribute to increased adhesion of the tip with the sample at those locations. Not all images in figure 4 were created with the same cantilever, which resulted in variations in stiffness and tip shape, which can also contribute to different adhesion between tip and sample. Overall, we concluded that the integrated actuator and sensor were suitable for imaging the cells in air, but the noise resolution was better in the case of optical detection attributed to the resistor readout, which in part can be attributed to the layout of the preamplifier board and the wiring.

3.2. Cantilever dynamics in fluid

The dynamics of the cantilever in air are distinctly different from the dynamics in fluid [24, 34, 31, 35–37]. The two main differences important to tapping mode AFM imaging are the reduction in resonance frequency and Q factor of the cantilever in fluid and the different mechanical coupling efficiencies of the tapping actuator to the surrounding medium. The latter is most significant in the case of the inertial drive of the

cantilever with an external tapping piezo. In air the coupling efficiency between the actuator (number 4 in figure 1(C)) to the cantilever chip (number 1 in figure 1(C)) is much more efficient than the coupling between the actuator and the surrounding air. The tuning curves in air therefore clearly show the resonance behavior of the cantilever and the curves for mechanical excitation and thermal excitation are nearly identical (figure 2 and the black curve in figure 5). When the cantilever is immersed in fluid, however, the coupling between the piezoactuator and the surrounding fluid becomes comparable to the coupling with the environment. Therefore the actuator excites many different resonances of the cantilever holder and the fluid, instead of exciting just the resonance of the cantilever. This results in the multitude of peaks in the tuning curve as shown in the orange curve in figure 5(A). This behavior has been thoroughly documented [34, 38] and several alternative actuation methods have been proposed to circumvent it, such as magnetic and Lorentz actuation [29, 25]. Here we show that the integrated thermal actuation is a well-suited method for exciting the cantilever at resonance in water, which is compatible with piezoresistive sensing. The blue curve in figure 5(A) shows clear resonances of multiple orders of the cantilever. When the cantilever is brought closer to the surface, damping between the cantilever and the surface increases and the resonance peak shifts further downward and decreases in Q factor (figure 5(B)).

3.3. Imaging in water

Figure 6 shows tapping mode images of a 10 μm pitch calibration grating in water with the active cantilevers using the four combinations of excitation and deflection readout. The thermal actuation used in figures 6(C) and (D) allows the exact

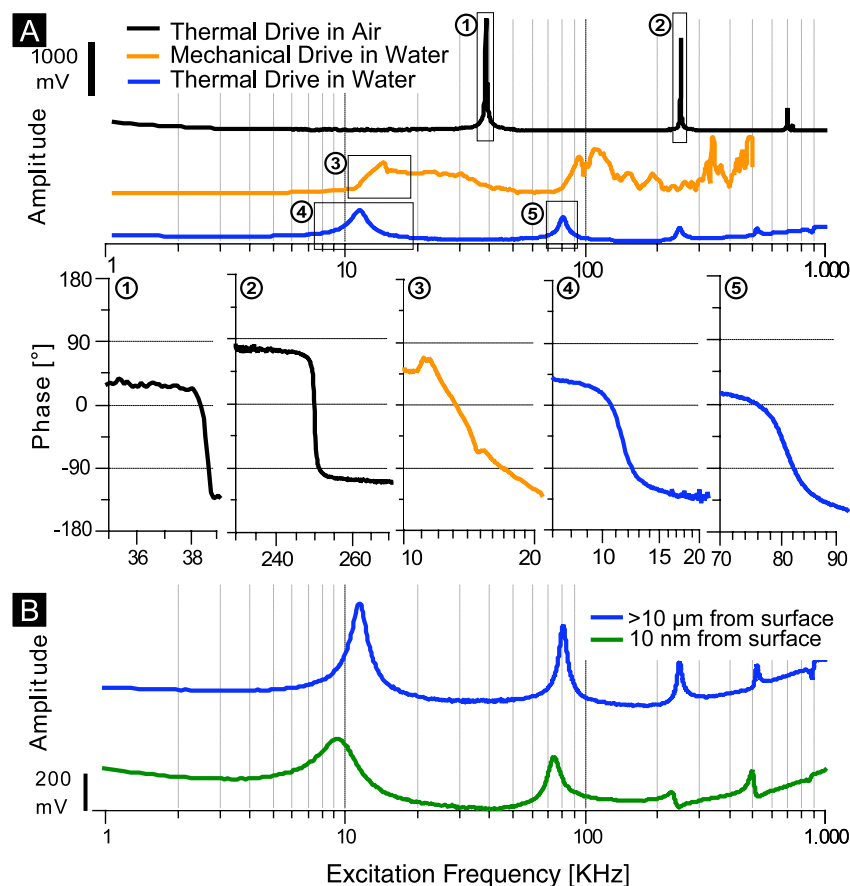


Figure 5. Excitation of resonances of the active cantilever in air and water using external inertial drive and integrated thermal actuator. (A) Amplitude curves of the cantilever excited with the thermal drive in air (black curve), the external inertial drive in water (orange curve) and the thermal drive in water (blue curve). The external inertial drive does not show clearly resolved resonance peaks, but rather a convolution of the resonances of the fluid cell and the resonance of the cantilever. The downward shift of the resonance peaks from air to water as well as the increased Q factor is apparent between the black and the blue curve. The Q factors of the cantilever in air and water are approx. 100 and approx. 5, respectively. Phase transitions of selected resonances are plotted underneath the amplitude curve, showing the clean tuning curve in the case of the thermal actuator compared to the inertial drive. (B) Amplitude tuning curves with thermal actuation retracted far from the surface (blue curve) and 10 nm off the surface (green curve). There is a notable shift of the resonance frequency to lower values as well as higher damping when the cantilever is close to the surface.

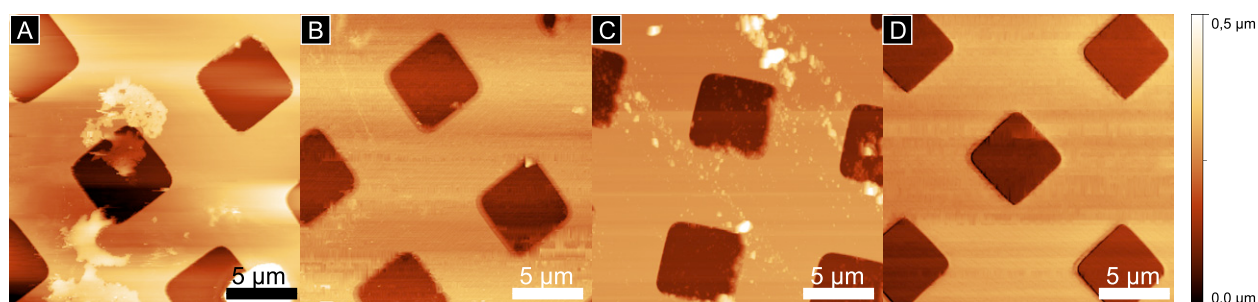


Figure 6. Images of 10 μm pitch calibration grating recorded in water using the four combinations of actuation and sensing. (A) Inertial drive and optical readout, (B) inertial drive and resistor readout, (C) thermal drive and optical readout and (D) thermal drive and resistor readout. Imaging was possible with all combinations. Low signal levels of the resistor signal resulted in a somewhat reduced image quality compared to the optical readout. Image D was recorded with excitation at half the resonance frequency while measuring the amplitude at the resonance frequency (2ω drive).

determination of the resonance frequency and the appropriate tapping frequency. The detection using piezoresistors yielded less detail in the images due to the lower signal-to-noise ratio. This manifests itself in water more than in air because

the frequency of the oscillation is less. Therefore, the time constant of the lock-in amplifier has to be increased in order to obtain stable amplitude detection, which reduces the detection bandwidth. When both the integrated thermal actuator and

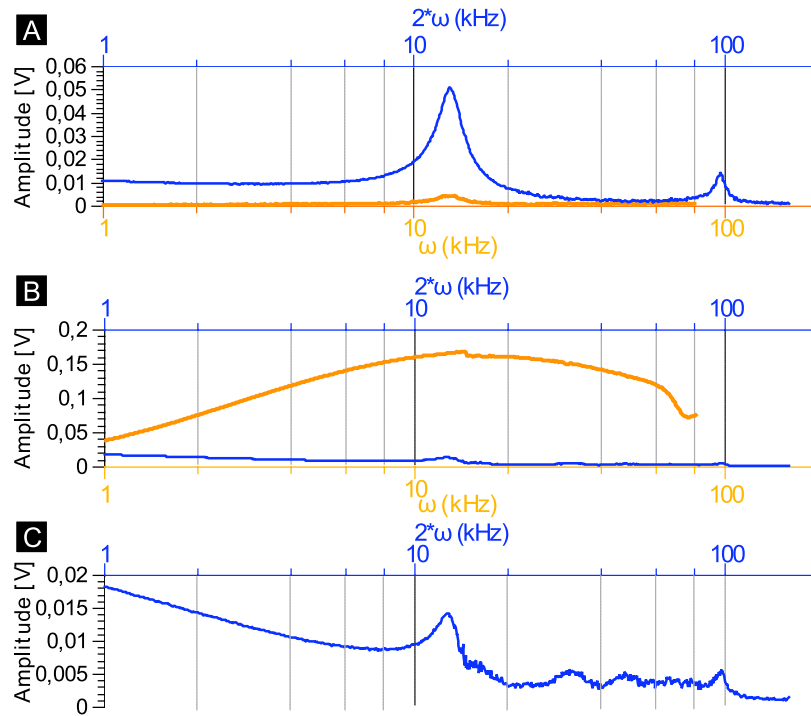


Figure 7. Frequency sweep curves with thermal actuation in water with detection of the amplitude at the excitation frequency ω and $2 * \omega$. (A) Amplitude tune using optical detection. The orange curve represents the amplitude detected at ω , when exciting at ω . The blue curve represents the amplitude detected at $2 * \omega$ when exciting at ω . (B) Amplitude tune using resistor detection. When detecting the amplitude at the same frequency as the excitation, the cross-coupling dominates the tuning curve obscuring the resonance signal (orange curve). The curve detected at $2 * \omega$ is much less obscured, making the mechanical resonance detectable and usable for imaging. (C) Zoom in of the 2ω curve from part (B).

the integrated resistive sensing is used (figure 6(D)) increased electrical cross coupling between the actuator and the sensor distort the detection of the cantilever resonance to a degree that no suitable resonance is present in the spectrum. The cross-coupling manifests itself in the deflection signal as a superposition of a scaled version of the drive signal onto the signal arising actually from the deflection of the cantilever. This cross-coupling can completely dominate the signal at higher drive currents (which are required for excitation in water). One way to avoid this issue is to take advantage of the nature of the thermal actuator. Since the thermal actuator bends as a result of heating, the deflection ($d(t)$) of the cantilever will be proportional to the power dissipated ($P(t)$):

$$\begin{aligned}
 d(t, \omega) &\propto P(t) \\
 P(t, \omega) &= \frac{V(t)^2}{R} \\
 V(t, \omega) &= A_0 \sin(\omega t) + B \\
 P(t, \omega) &= \frac{A_0^2}{R} \left(\frac{1 - \cos(2\omega t)}{2} \right) + \frac{2A_0 B}{R} \sin(\omega t) + \frac{B^2}{R} \\
 d(t, \omega) &= \frac{1}{R} \left\{ \underbrace{2A_0 B \sin(\omega t)}_{\text{for excitation at } \omega_{n1}} - \underbrace{\frac{A_0^2}{2} \cos(2\omega t)}_{\text{for excitation at } \omega_{n1}/2} \right. \\
 &\quad \left. + \underbrace{\left(B^2 + \frac{A_0^2}{2} \right)}_{\text{for low frequency deflection}} \right\}
 \end{aligned} \tag{1}$$

where $P(t, \omega)$ is the electrical power, $V(t, \omega)$ is the drive voltage, R is the heater resistance, A_0 is the drive amplitude, ω is the drive frequency, B is the DC offset, $d(t, \omega)$ is the cantilever deflection and ω_{n1} is the first eigenfrequency of the cantilever.

Equation (1) shows that, for a voltage applied to the cantilever given by $V(t, \omega) = A_0 \sin(\omega t) + B$, the cantilever gets excited at the frequencies ω and 2ω . This allows for the separation of the excitation signal and the detection signal in the frequency domain. When the constant offset $B = 0$, the ω part of the excitation disappears and the cantilever will only be excited at 2ω . Any residual signal component at ω will then be from electrical cross-coupling and not from actual motion of the cantilever. Figure 5(A) shows the effectiveness of the 2ω drive. When excited at ω and detected at ω with $B = 0$, only a small peak can be seen at the resonance frequency at ≈ 13 kHz (orange curve in figure 7(A)). However, when exciting at ω and detecting at 2ω , the first and second eigenfrequency of the cantilever can be seen clearly (blue curve in figure 7(A)). Figure 7(B) shows the same experiment with resistor readout of the deflection. When exciting and detecting the deflection at the same frequency, the coupling completely dominates the signal (as can be seen from the large amplitude of the orange curve). When exciting at ω and detecting at 2ω , however, the cross-coupling is drastically reduced and the resonance peak is clearly discernible (blue curve in figures 7(B) and (C)). Although the coupling has been reduced significantly, some residual cross-coupling remains (as is evident from the

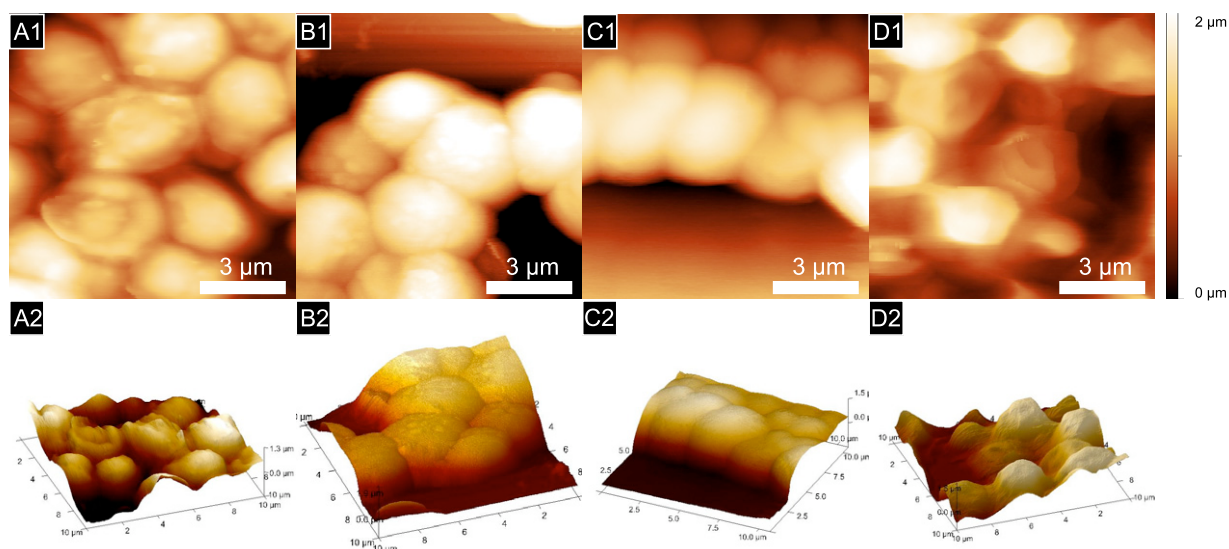


Figure 8. Tapping mode images of yeast cells recorded in water imaged with active cantilevers and the four actuation/detection combinations. (A) Inertial drive and optical readout. (B) inertial drive and resistor readout, (C) thermal drive and optical readout. Image D was recorded using thermal drive and resistor readout with 2ω drive (excitation at half the resonance frequency while measuring the amplitude at the resonance frequency). The upper row of images shows the height data, while the lower row of images shows 3D representation of mixed height and amplitude data.

presence of a non-zero amplitude below the resonance). We attribute this to two factors. First, the Q factor of the cantilever resonance is low and the excitation of both the ω as well as the 2ω term can be excited with a single excitation frequency. As a second factor we expect that the 3 dB point of the actuation bandwidth of the integrated cantilever is of the same order of magnitude as the cantilever resonance [30]. The cantilever will therefore also be deflected at frequencies below the resonance frequency.

Figure 6(D) was recorded by exciting at ω and using the amplitude of the resistor signal at 2ω as input to the PI feedback loop.

To see if the actuated cantilevers can be used for imaging soft biological samples in fluid, we imaged yeast samples rehydrated in water using the four combinations of actuation and sensing (figure 8). Acquiring images A–C of figure 8 required no significant modifications for the sample (compared to figure 4) or the imaging procedure (compared to figures 6(A)–(D)). This showed that the actuator as well as the sensor have enough stability and sensitivity to operate on soft biological samples. In the case where both the integrated actuator and sensor were used (figure 8(D)), complications arose from excessive forces exerted by the cantilever on the samples. We attribute these high force interactions to the remaining electrical coupling between actuation and sensing, which reduces the slope of the resonance peak below the resonance frequency (see figure 7(C)). This effect becomes more pronounced when the damping of the cantilever increases near the surface. This increased imaging force resulted in deformation and detachment of the yeast cells from the polylysine-covered glass slides. We therefore changed the sample preparation by cross-linking the cells with glutaraldehyde. This increased the stiffness of the cells as well

as their interconnectivity which made it possible to image the cells using both integrated sensing and actuation. This cross-linking, however, might not be suitable for applications where it is important that the surface chemistry of the yeast is not altered.

4. Discussion

The experimental data presented in this paper shows that active cantilevers with integrated thermal micro-actuator and resistive sensor can be operated in tapping mode in water. While the resistive sensing in our current cantilever design when used in fluid does not achieve the same noise levels as the optical lever detection, it is sufficient to image both hard and soft samples in fluid with good quality. We believe that the noise arises from the sensor itself as well as from the electronics and the wiring layout in our specific set-up. Since it has been shown that the piezoresistive readout of cantilevers in air can achieve equal performance to the optical lever detection, we are confident that future improvements in cantilever design and electronic layout will also decrease the noise of the detection mechanism when operated in fluid. The thermal actuation of the cantilever shows significant improvements for actuation in fluid compared to the external inertial drive with a tapping piezo. In some cases, uncoated cantilevers showed interaction with the water after prolonged use. In one case, bubble formation occurred on the cantilever when actuated. Three possible effects could be responsible for this: (1) outgassing of the cantilever due to heating, (2) cavitation or (3) electrolysis. We believe the latter to be responsible, but were unable to reproduce this effect. On one particular sample (a heavily used calibration grating), material built up on the cantilever from the solution or sample. We speculate that this was due

to electrostatic interactions of the contaminating material with the heater. Thorough cleaning of the calibration grating solved this, but it should be noted that some materials can be attracted to the cantilever. The exact mechanism and possible solutions are subject to ongoing investigation.

The cross-coupling between actuation and sensing is the dominant problem when using both the integrated actuator and sensor for imaging in water. The excitation at ω and detection at 2ω is a promising way to circumvent this problem, but two issues remain. When the cross-coupling dominates the sensor signal and the actual deflection is only a small signal on the larger carrier wave, the gain of the preamplifiers are easily saturated without reaching the desired signal levels after the lock-in amplifier detecting at 2ω . The second issue is that the excitation at 2ω requires higher peak currents in the form of A_0 (see equation (1)). This could reduce the lifetime of the actuator. We therefore believe that reducing the cross-coupling through cantilever and electronic design would be most desirable.

The cantilevers used in this study have resonance frequencies and spring constants optimized for operation in air. In a next-generation cantilever, we will attempt to decrease the spring constant to below 0.5 N m^{-1} to make the cantilevers better suited for imaging soft biological samples. Another factor that contributed to the difficulty for accurate detection using both the integrated actuator as well as the sensor is the low Q factor of the resonance, especially when close to the surface. This is amplified by the low tip height of our cantilevers ($\approx 4 \mu\text{m}$). Increasing the tip height in a new design will improve this.

5. Conclusion

In this paper we have performed tapping mode atomic force microscopy imaging in fluid using fully instrumented cantilevers that combine integrated thermal micro-actuators and piezoresistive deflection sensors. When using either the thermal actuator or the resistive sensor in combination with a traditional sensor or actuator, respectively, most commercially available AFM and feedback schemes can be used. When using both the integrated actuator and sensor at the same time, better performance is achieved when using the frequency-doubling characteristic of the thermal actuator to actuate the cantilever with ω and detect the amplitude at 2ω using a lock-in amplifier. Accurate imaging of rehydrated yeast cells shows the potential of this approach for making fully integrated active cantilevers designed specifically for imaging in fluid. Such cantilevers will significantly ease automation of biological AFM imaging in fluid and could contribute to extending the use of AFM to routine biomedical and medical diagnostic applications.

Acknowledgments

The authors gratefully acknowledge the help of Pat McPhail from Veeco Metrology Inc., Santa Barbara, CA and Vladimir Stavrov of NTS, Botevgrad, Bulgaria. This work was funded by the Army Research Office, Institute for Collaborative Biotechnologies, by the National Institute of Health under

Award RO1 GM065354 and by the Austrian Research Promotion Agency under award no. VO156-08-BII: NSI-FABICAN. GEF is supported by a Schrödinger fellowship J2778-B12. WS is supported by a DAAD fellowship D/08/50444.

References

- [1] Ukraitsev V A, Baum C, Zhang G and Hall C L 2006 The role of AFM in semiconductor technology development: the 65 nm technology node and beyond *Proc. SPIE* **5752** 127–39
- [2] Tang Q, Shi S Q and Zhou L M 2004 *J. Nanosci. Nanotechnol.* **4** 948–63
- [3] Sun X P, Zhang B L and Wang E K 2003 *Chin. J. Anal. Chem.* **31** 1127–30
- [4] Allen S, Rigby-Singleton S M, Harris H, Davies M C and O'Shea P 2003 *Biochem. Soc. Trans.* **31** 1052–7
- [5] Dufrene Y F 2004 *Nat. Rev. Microbiol.* **2** 451–60
- [6] Muller D J and Dufrene Y F 2008 *Nat. Nanotechnol.* **3** 261–9
- [7] Muller D J, Helenius J, Alsteens D and Dufrene Y F 2009 *Nat. Chem. Biol.* **5** 383–90
- [8] Foster B 2009 *Am. Lab.* **41** 11–3
- [9] Lekka M and Laidler P 2009 *Nat. Nanotechnol.* **4** 72
- [10] Bolshakova A, Kiselyova O and Yaminsky I 2004 *Biotechnol. Prog.* **20** 1615–22
- [11] Parot P, Dufrène Y F, Hinterdorfer P, Grimellec C L, Navajas D, Pellequer J L and Scheuring S 2007 *J. Mol. Recognit.* **20** 418–31
- [12] Albrecht T R, Akamine S, Carver T E and Quate C F 1990 *J. Vac. Sci. Technol. A* **8** 3386–96
- [13] Lee K L, Abraham D W, Secord F and Landstein L 1991 *J. Vac. Sci. Technol. B* **9** 3562–8
- [14] Sadewasser S, Villanueva G and Plaza J A 2006 *Rev. Sci. Instrum.* **77** 073703
- [15] Lee D W, Ono T and Esashi M 2000 *Sensors Actuators A* **83** 11–16
- [16] Linnemann R, Gotszalk T, Rangelow I W, Dumania P and Oesterschulze E 1996 *J. Vac. Sci. Technol. B* **14** 856–60
- [17] Alexander S, Hellemans L, Marti O, Schneir J, Elings V, Hansma P K, Longmire M and Gurley J 1989 *J. Appl. Phys.* **65** 164–7
- [18] Putman C A J, Grooth B G D, Hulst N F V and Greve J 1992 *J. Appl. Phys.* **72** 6–12
- [19] Ohnesorge F and Binnig G 1993 *Science* **260** 1451–6
- [20] Walters D A, Cleveland J P, Thomson N H, Hansma P K, Wendman M A, Gurley G and Elings V 1996 *Rev. Sci. Instrum.* **67** 3583–90
- [21] Viani M B *et al* 1999 *Rev. Sci. Instrum.* **70** 4300–3
- [22] Tortonese M, Barrett R C and Quate C F 1993 *Appl. Phys. Lett.* **62** 834–6
- [23] Rogers B, York D, Whisman N, Jones M, Murray K, Adams J D, Sulchek T and Minne S C 2002 *Rev. Sci. Instrum.* **73** 3242–4
- [24] Florin E L, Radmacher M, Fleck B and Gaub H E 1994 *Rev. Sci. Instrum.* **65** 639–43
- [25] Han W, Lindsay S M and Jing T 1996 *Appl. Phys. Lett.* **69** 4111–3
- [26] Lantz M A, O'Shea S J and Welland M E 1994 *Appl. Phys. Lett.* **65** 409–11
- [27] Revenko I and Proksch R 2000 *J. Appl. Phys.* **87** 526–33
- [28] Pedrak R, Ivanov T, Ivanova K, Gotszalk T, Abedinov N, Rangelow I W, Edinger K, Tomerov E, Schenkel T and Hudek P 2003 *J. Vac. Sci. Technol. B* **21** 3102–7
- [29] Buguin A, Roure O D and Silberzan P 2001 *Appl. Phys. Lett.* **78** 2982–4

- [30] Fantner G, DJB, Youcef-Toumi K, Belcher A and IWR 2009 *Trans. ASME J. Dyn. Syst. Meas. Control* at press
- [31] Herruzo E T and Garcia R 2007 *Appl. Phys. Lett.* **91** 143113
- [32] Ivanov T, Gotszalk T, Grabiec P, Tomerov E and Rangelow I W 2003 *Microelectron. Eng.* **67/68** 550–6
- [33] Boder E T and Wittrup K D 2000 *Methods Enzymol.* **328** 430–44
- [34] Hansma P K *et al* 1994 *Appl. Phys. Lett.* **64** 1738–40
- [35] Jai C, Cohen-Bouhacina T and Maali A 2007 *Appl. Phys. Lett.* **90** 113512
- [36] Maali A, Hurth C, Cohen-Bouhacina T, Couturier G and Aime J P 2006 *Appl. Phys. Lett.* **88** 163504
- [37] Weisenhorn A L, Hansma P K, Albrecht T R and Quate C F 1989 *Appl. Phys. Lett.* **54** 2651–3
- [38] Putman C A J, d Werf K O V, Grooth B G D, Hulst N F V and Greve J 1994 *Appl. Phys. Lett.* **64** 2454–6